Advanced Composites and Hybrid Materials (2023) 6:89
https://doi.org/10.1007/s42114-023-00657-w

RESEARCH

Construction of reliable ion-conducting channels based on the perfluorinated anion-exchange membrane for high-performance pure-water-fed electrolysis

Shuhong Zheng[1] · Shengqiu Zhao[1] · Hongyun Tan[1] · Rui Wang[1] · Miaoyan Zhai[1] · Haining Zhang[1,3] · Huali Qin[2] · Haolin Tang[1,3]

Received: 15 February 2023 / Revised: 13 March 2023 / Accepted: 20 March 2023

Abstract
Constructing reliable ion transport channels is an effective strategy of achieving equal hydroxide conductivity and physical stability in anion-exchange membranes (AEMs). Herein, a series of perfluorinated anion exchange polymers terminated with trimethyl ammonium cations (Cn-PFTMA ($n = 2, 4, 5$)) with different carbon ether side chains were synthesized from dissoluble perfluorosulfonic acid ionomers. These Cn-PFTMA membranes feature a unique microphase structure, enabling them to maintain a high hydroxide conductivity even at low ion exchange capacities (IEC), while avoiding physical stability deterioration due to excessive water absorption and swelling from high IEC. At 80 °C, the C2-PFTMA membrane with a very low IEC value of 1.20 meq g^{-1} presents a hydroxide conductivity of 94.7 mS cm^{-1}, 1.8 times higher than that of the commercial FAA-3-50 membrane (IEC = 1.89 meq g^{-1}). As a result, water electrolysis with the C2-PFTMA membrane has achieved an impressive performance of 277 mA cm^{-2}@1.9 V when supplied with pure water. This research provides a viable strategy for achieving equal hydroxide conductivity and physical stability of AEMs.

Keywords Perfluorinated ionomers · Anion exchange membranes · Microphase separation structure · Hydroxide conductivity · Physical stability

1 Introduction

Water electrolysis of hydrogen is a key element of the green energy transition [1]. The development of anion exchange membrane water electrolysis (AEMWE) technology has the potential to combine the cost-effectiveness of alkaline water electrolysis (AWE) with the convenience, efficiency, and rapid response of proton exchange membrane water electrolysis (PEMWE). This technology eliminates the need for precious metal catalysts and titanium components and can operate under different pressures [2–4]. However, the anion exchange membrane, which is a key component of the electrolyzer, has hindered further progress due to its low hydroxide conductivity and durability [5, 6].

In recent years, aromatic polyelectrolytes such as polybenzimidazole, polystyrene, polyethersulfone, and polyetheretherketone, have attracted considerable attention among researchers and were once thought to be suitable as AEM materials [7–12]. Unfortunately, the rigid C–C bond in the polyaromatic polymer, which provides AEMs with excellent strength, significantly decreases the water uptake and adversely affects the hydroxide conductivity. It is essential to find a balanced approach to achieve desirable hydroxide conductivity and physical stability of AEMs. Although the hydroxide conductivity of AEMs can be improved by increasing the IEC, excessive hydration swelling and carbonation of AEMs induced by a high IEC might compromise the

Shuhong Zheng and Shengqiu Zhao contributed equally to this work.

✉ Haolin Tang
thln@whut.edu.cn

[1] State Key Laboratory of Advanced Technology for Materials Synthesis and Processing, Wuhan University of Technology, Wuhan 430070, China

[2] School of Chemistry, Chemical Engineering and Life Sciences, Wuhan University of Technology, Wuhan 430070, China

[3] Foshan Xianhu Laboratory of the Advanced Energy Science and Technology Guangdong Laboratory, Xianhu Hydrogen Valley, Foshan 528200, China

Published online: 20 April 2023

physical stability [13]. Manabu Tanaka et al. discovered that multi-block copolymer membranes exhibited higher hydroxide conductivity than random copolymer membranes, demonstrating that microphase separation effectively enhanced the hydroxide conductivity of AEMs without sacrificing its physical stability, providing a new approach for the design of AEMs [14]. But large amounts of $–CH_2–$ spacers are present in both the polymer backbone and the side chains as described above, making the development of a well-apparent hydrophobic phase more challenging due to the poor polarity difference between hydrocarbon-based alkyl chains and hydrophilic ion groups [15].

Perfluorinated ionomers, a class of polymers consisting of a hydrophobic tetrafluoroethylene backbone and hydrophilic fluoroalkyl side chains that can easily form phase separation structures to facilitate ion transport, are widely utilized due to their remarkable stability and ion conductivity [16–18]. Additionally, perfluorinated ionomers possess low water absorption due to their highly hydrophobic tetrafluoroethylene body backbone, which is deemed to be essential for preserving the physical stability of the membrane [19–21]. As a result, perfluorinated ionomers are seen as a potential substitute to AEM materials due to their advantageous properties.

Researchers have made significant efforts to create more advanced AEM materials. Several studies have been conducted to synthesize perfluorinated AEMs (PFAEMs) made from perfluorosulfonyl fluoride ($PFSO_2F$) precursor modification, which have been found to have well-driving phase separation and physical stability. PFAEMs have been studied for their potential in the synthesis of $PFSO_2F$ with 1,4-dimethylpiperidine and have been compared to hydrocarbon AEMs in the same cation. Results have shown that the perfluorinated backbone allows for a minimum threefold reduction in water absorption while still providing a significant improvement in hydroxide conductivity [22]. The applicability of perfluorinated materials in the field of AEMs has been demonstrated and has great potential for further development. Additionally, PFAEMs with the chemical architecture identical to Nafion® using nphenylhydroxylamine (NR-HPA) prepared via $PFSO_2F$ and phenylhydroxylamine have been studied, but unfortunately, NR-HPA with a conducting hydroxide group of secondary amine cation presented poor hydroxide conductivity and AEMWE performance at 80 °C, likely due to weak ionization of the secondary amine structure cationic groups [23]. In contrast, PFAEMs containing quaternary ammonium cation groups (S-$PFSO_2NH$-GCI-OH) were synthesized from $PFSO_2F$ and glycidoxypropyltrimethylammonium chloride, resulting in a conductivity of up to 10^2 mS cm^{-1} due to the high ionization constant of the cations [24]. Additionally, these quaternary ammonium cations are advantageous for their effective synthesis and robustness in alkaline conditions [25].

Herein, quaternary ammonium PFAEMs were synthesized from soluble perfluorosulfonic acid polymers with varying side chain lengths via acid–base and alkylation reactions with liquid ammonia and iodomethane. This enabled the construction of reliable ion channels due to the unique microphase structure of the perfluorinated ionomer, which facilitated rapid hydroxide ion transport at low water uptake. As such, Cn-PFTMA ($n = 2, 4, 5$) membranes demonstrated excellent hydroxide conductivity at low IEC, thus avoiding the physical stability issues caused by excessive water absorption and swelling. Additionally, the side chain length had an effect on the microphase separation of AEMs, with the volume of hydrophilic channels increasing with the length of the side chains. While density functional theory (DFT) calculations were performed to further investigate the impact of side chain length on cationic groups. As a result, the properties of Cn-PFTMA were evaluated in terms of electrochemical properties, physical and chemical stability, and water electrolysis properties. This research provides new insights into the development of AEMs with combined superior hydroxide conductivity and physical stability.

2 Experimental

2.1 Materials

The perfluorosulfonic acid ionomer ($PFSO_3H$) with two carbon ether side chains (D79, EW = 790 g eq^{-1}, marked as C2-$PFSO_3H$) was obtained from Solvay Company. The $PFSO_3H$ with four carbon ether side chains (3 M, EW = 800 g eq^{-1}, marked as C4-$PFSO_3H$) was obtained from 3 M Company. The $PFSO_3H$ with five carbon ether side chains (D2020, EW = 1100 g eq^{-1}, marked as C5-$PFSO_3H$) was obtained from DuPont Company. Iodomethane and cesium carbonate were purchased from J&K Scientific, Ltd. Ethyl acetate, isopropyl alcohol, ethanol, *N*, *N*-dimethylformamide (DMF), and potassium hydroxide (KOH) were purchased from Sinopharm Chemical Reagent Co., Ltd. Alkaline membrane (Fumapem FAA-3-50) and alkaline ionomer (Fumapem FAA-3) were purchased by Fuel Cell Store (USA).

2.2 Polymer functionalization

2.2.1 Synthesis of perfluorosulfonamide (Cn-$PFNH_2$)

The Cn-$PFNH_2$ was synthesized by the acid–base reaction between the sulfonic group and liquid NH_3 and heat-induced dehydration (Scheme 1). Concretely, Cn-$PFSO_3H$ (10.0 g) with excess liquid NH_3 reacted for 4 h at − 40 °C. After the final reaction, the system was slowly heated

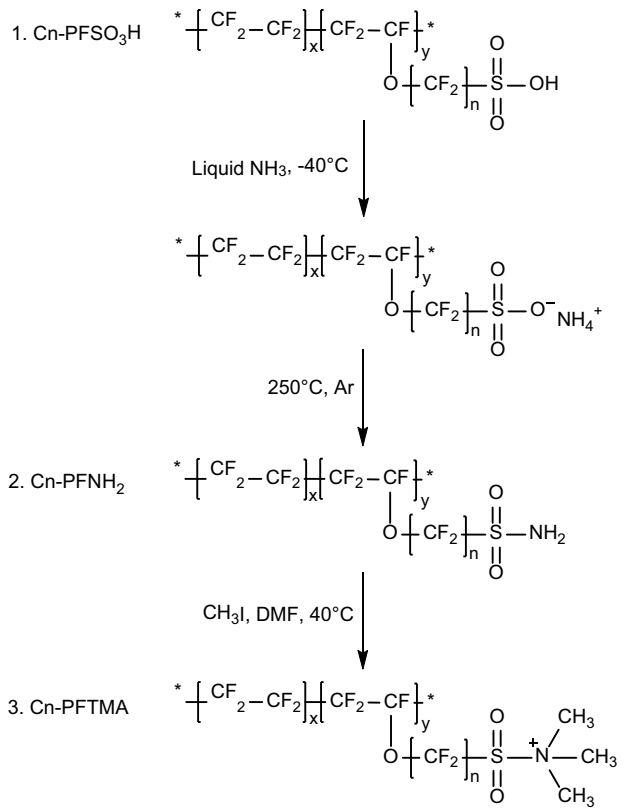

Scheme 1 Synthetic route of Cn-PFTMA

to room temperature, and the residual NH_3 was released entirely. Subsequently, the sample was treated at 250 °C for 90 min under a continuous Argon atmosphere.

2.2.2 Synthesis of quaternary ammonium perfluorinated anion exchange polymer (Cn-PFTMA)

The synthesis of C2-PFTMA, C4-PFTMA, and C5-PFTMA was achieved through an alkylation reaction. To begin, a mixture of C2-$PFNH_2$ (10.0 g) and cesium carbonate (8.3 g) was added to DMF (157.0 g) to form a 10.5 wt% system. After stirring at room temperature for 1 h, iodomethane (18.0 g) was added dropwise, and the reaction was allowed to proceed at 40 °C for 48 h in the dark. Upon cooling to room temperature, the product was precipitated in ethyl acetate and filtered to remove excess iodomethane, followed by repeated washing with ethanol and deionized water via centrifugation at 5000 rpm to eliminate the residual ethyl acetate and cesium carbonate. Finally, the sediment was dried under a refrigerated vacuum to obtain a white powder (C2-PFTMA). The same procedure was applied to synthesize C4-PFTMA and C5-PFTMA, yielding a light brown powder.

2.3 Membrane preparation

The Cn-PFTMA membranes were prepared by the flow-casting method. 1.0 g Cn-PFTMA powder was dissolved in a 16.0 g mixture of deionized water and isopropyl alcohol (6:4) at 130 °C, and the solution was cooled to 25 °C. The solution was poured onto a flat glass plate (10 × 10 cm) and maintained at 55 °C for 10 h, followed by annealing at 220 °C for 2 h. The membrane was then peeled off the glass plate with a thickness of approximately 50 ± 2 μm. Finally, the membrane was immersed in 1 M KOH solution overnight at 25 °C to exchange the I^- anions with OH^- anions via anion exchange.

2.4 Characterization of polymers and membranes

NMR was conducted using a Bruker Avance III 400 M spectrometer operating at 500 MHz for ^{1}H NMR in DMSO-d_6. FT-IR spectra in the range of 4000–400 cm^{-1} was obtained on a Thermofisher Scientific Nicolet6700 spectrometer. The dispersion characteristic of the ionomers was evaluated at 25 °C with a Brookhaven BI-90Plus dynamic light scattering (DLS) device, with the sample solutions being diluted to 0.1 wt%. The surface morphology of the membrane was studied using a Seiko SPA400 atomic force microscope (AFM) in tapping mode, after moisturizing the membrane for 3 h at 100% relative humidity (RH). The microstructure was analyzed by Xenocs Xeuss3.0 small-angle X-ray (SAXS) after moisturizing the samples for 3 h under 100% RH.

2.4.1 IEC

To measure the ion exchange capacity (IEC), the inverse titration method was employed. The OH^- form membrane samples were weighed after drying, and then soaked in 50 mL of 0.01 M HCl solution for 2 days. To analyze the acid usage, the 0.01 M KOH solution with phenolphthalein was applied. The IEC of the membrane samples was calculated using the Eq. (1):

$$IEC = \frac{V_{HCl}M_{HCl} - V_{KOH}M_{KOH}}{W_{dry}} \quad (1)$$

where V_{HCl} and M_{HCl} are the volume and concentration of the HCl solution, respectively; V_{KOH} and M_{KOH} are the volume and concentration of the KOH solution, respectively; and W_{dry} is the weight of the dried sample.

2.4.2 WU and V_S

The OH^- form membrane samples were sliced into 2 × 2 cm rectangular blocks. Then, the experiments were performed in deionized water under variable conditions of 1 h and relative

temperatures (30, 40, 50, 60, 70, and 80 °C, respectively). Then, the samples were measured quickly to obtain their weight, length, and thickness after drying the surface moisture. Afterward, the sample membranes were heat-treated at 60 °C to record weights. The water uptake (WU) and volume swelling ratio (V_S) of membrane samples were acquired using the Eqs. (2) and (3):

$$WU = \frac{W_{wet} - W_{dry}}{W_{dry}} \times 100\% \tag{2}$$

$$V_s = \frac{V_{wet} - V_{dry}}{V_{dry}} \times 100\% \tag{3}$$

where W_{wet} and W_{dry} are the weights of the wet and dry membrane samples, respectively; and V_{wet} and V_{dry} are the volumes of the wet and dry sample membranes, respectively; and the volume is calculated as the length × width × thickness.

2.4.3 Hydroxide conductivity

The alternating current (AC) impedance measurement method was adopted to evaluate the hydroxide conductivity of the sample membranes from 1 MHz to 0.1 Hz via Metrohm Autolab 302N electrochemical test system. The impedance curve was obtained under varying circumstances of relative humidity and temperature. The hydroxide conductivity was calculated according to Eq. (4):

$$\sigma = \frac{D}{R \times L \times T} \tag{4}$$

where D is the distance between the two electrodes, R is the ohmic resistance analyzed from the impedance curve, and L and T are the width and thickness of the sample membranes, respectively.

2.4.4 Stability and mechanical property

The thermal stability of the samples was tested via STA 449F3 under argon with a heating rate of 10 °C min^{-1} from 20 to 800 °C. A tensile measurement (ETH-080ST-SSP) was employed to evaluate the tensile strength of the sample membranes. The samples were cut into 8 × 10 cm sizes, while the tensile rate was set to 10 mm min^{-1}.

2.4.5 Theoretical calculations

Gaussian (G16) suite of program was adopted to conduct density functional theory (DFT) calculations with Becke's three-parameter hybrid method using the Lee-Yang-Parr correlation functional (B3LYP). The geometrical structures and the vibrational modes were calculated at 6-31G (d) level. The electrostatic potential (ESP), the lowest unoccupied molecular orbital (LUMO), and the highest occupied molecular orbital (HOMO) of each repeating unit were obtained after optimized.

2.4.6 MEA preparation and electrolysis performance tests

The synthesized Cn-PFTMA and commercial FAA-3-50 membranes were employed for the anion-exchange membranes. The C2-PFTMA ionomer and FAA-3 ionomer were dissolved in a mixed solution of deionized water and isopropanol (6:4) to prepare a 5 wt% ionomer solution. Subsequently, the anode catalyst ink was prepared by combining IrO_2 (Kaida), isopropyl alcohol, distilled water, and either the C2-PFTMA or FAA-3 ionomer; the cathode ink was prepared by 50 wt% Pt/C (Tanaka Kikinzoku Kogyo), isopropyl alcohol, distilled water, and either the C2-PFTMA or FAA-3 ionomer, which were then mixed together using ball milling and sonication for 2 h, respectively. Finally, the catalyst ink was sprayed onto the membrane using nitrogen gas to form a membrane electrode assembly (MEA) with an active area of 25 cm^2, and the loading of IrO_2 in the anode and Pt in cathode was 1.8 mg cm^{-2} and 0.4 mg cm^{-2}, respectively. A homemade anion-exchange membrane water electrolyzer was employed to evaluate the performance of Cn-PFTMA. The reactant used was deionized water at a temperature of 70 °C, with the anode and cathode fed at a rate of 5 mL min^{-1}. The MEAs were activated by applying a high voltage of 1.85–1.95 V until the current was stabilized. The polarization curves were obtained by applying a step voltage (1.4–2.0 V) for a fixed time of 10 min in constant potential mode. An IPS PTC-05100EW potentiostat was used to measure the EIS at 1.9 V, with a frequency range of 100 kHz to 0.1 Hz and an amplitude of 0.95 mV [26, 27].

3 Results and discussion

3.1 Synthesis and characterization of the Cn-PFTMA polymers

Cn-PFTMA was synthesized through an acid–base reaction, followed by thermal-induced dehydration and alkylation, as shown in Scheme 1. The structure of the obtained Cn-$PFNH_2$ and Cn-PFTMA were identified utilizing ^{1}H NMR spectroscopy and FT-IR spectra, depicted in Figs. 1 and S1. As the ^{1}H NMR spectroscopy of C2-PFTMA is shown in Fig. 1a, a characteristic peak at 7.06 (^{b}H) ppm was observed in the C2-$PFNH_2$, while the characteristic peaks at 4.37 (^{a}H) ppm attributing to the –SO_3H proton (H^a) completely disappeared, which proved that the C2-$PFNH_2$ was successfully

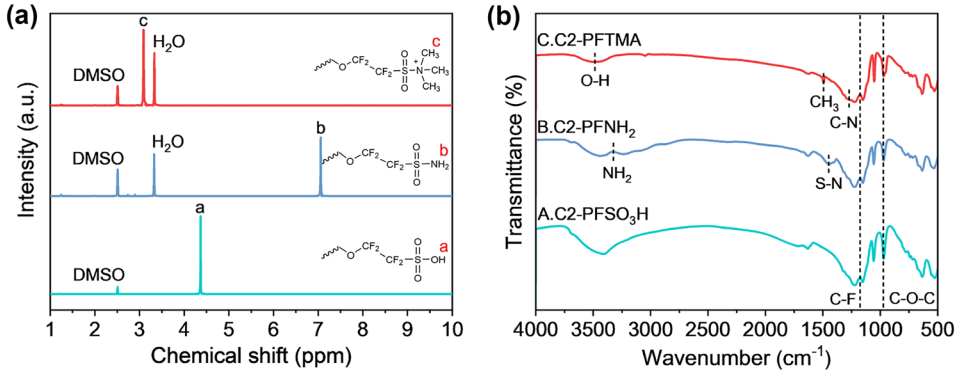

Fig. 1 **a** ^{1}H NMR spectra and **b** FT-IR spectra of C2-PFSO$_3$H, C2-PFNH$_2$, C2-PFTMA

synthesized. After alkylation and quaternization, the diamine signal disappeared, and the new peak appeared at 3.09 (^{c}H) ppm assigned to –N–CH$_3$ (H^{c}) in the C2-PFTMA, indicating the successful preparation of C2-PFTMA. Moreover, the C–H in the quaternary ammonium cation exhibited a higher chemical shift could be attributed to the electron deficiency of –N^{+} [7]. C4-PFTMA and C5-PFTMA presented a similar chemical shift to C2-PFTMA. The slight shift of the peaks might be due to different side chain lengths (Fig. S1).

C2-PFTMA was further characterized by FT-IR (Fig. 1b). The raw material spectrum of C2-PFSO$_3$H showed the original signals, including the C–O–C appearing at 968 cm^{-1}, and the stretching vibration of C–F is visible at 1150–1320 cm^{-1}, which was so strong that it covered other signals [28]. Compared to the C2-PFSO$_3$H, the typical signals at 3240–3430 cm^{-1} belonging to the twin amino group and at 1631 cm^{-1} related to the asymmetric N–H, and the peaks of the S–N band at 1448 cm^{-1} were observed, confirming the formation of the –SO$_2$NH$_2$ [29]. Moreover, the vibration peaks of C–O–C and C–F in C2-PFNH$_2$ were consistent with those in C2-PFSO$_3$H, demonstrating the acid–base response only proceeded for the sulfonic acid group and liquid NH$_3$ [30]. After the H on the diamine replacing by methyl, the disappearance of the diamine peak, the feature signals for C2-PFTMA, including the peaks for the C–H stretching and bending of CH$_3$, the stretching of O–H band, and C–N band at 3047 cm^{-1} and 1047 cm^{-1}, 3485 cm^{-1}, and 1271 cm^{-1}, respectively, confirmed the successful alkylation and quaternization of the amine [31, 32].

Uniform and fine particles of the resin polymer dispersion are essential for forming polyelectrolyte membranes with uniform thickness, homogeneous properties, and favorable microscopic morphology. The Cn-PFTMA ionomer exhibited good solubility in a mixed solution of water and isopropanol as a clear solution. The behavior of the particle size distribution of the Cn-PFTMA solutions and commercially available Fumatech FAA-3 dispersions is revealed in Fig. S2. In line with commercial resin dispersions, the particle size of all ionomer dispersions is less than 10^3 nm. Previous studies conducted by our group have highlighted that dispersions with uniform particle size distribution can significantly influence the orderly arrangement of microscopic ionic clusters in membranes [33]. Thus, it is likely that Cn-PFTMA membranes will demonstrate a similar property.

3.2 Morphology structure of the Cn-PFTMA membranes

A well-established microphase separation structure is essential for constructing reliable ion channels that accelerate the delivery of hydroxide [34–36]. Hence, SAXS was used to explore the microstructure because of the incompatibility of hydrophobic segments and hydrophilic clusters. Figure 2 presents the SAXS curves of Cn-PFTMA and FAA-3-50; there are two scattering peaks in the Cn-PFTMA profiles indicating the main-chain PTFE structure and the size of the ionic clusters [37]. Cn-PFTMA with increased side chain length revealed apparent diffraction peaks at 2.67 nm^{-1}, 2.65 nm^{-1}, and 2.61 nm^{-1}, corresponding to d-spacing of 2.35 nm, 2.37 nm, and 2.41 nm, respectively, calculated by the Bragg equation ($d = 2\pi/q$). Noteworthy, the scattering peak of C5-PFTMA is the most obvious and broadest, benefiting the formation of well-distinct phase separation morphology, as a feature of the long side chain structure. The phase separation performance of the random-structured FAA-3-50 was different from the Cn-PFTMA as there was only one diffuse broad peak in the SAXS curve. This phenomenon is further found directly from the 2D SAXS plots with a diffuse scattering ring (Fig. 2c). The evident scattering rings indicated the periodic distance (d) associated with the behavior of phase separation intra-brane. It became more distinct with increased side chain length. Consequently, as-prepared membrane with long side chain structure helps to develop a better microphase separation morphology and form a more fantastic ion channel which can accelerate the transport of hydroxide ions.

AFM images were employed further to confirm the hydrophilic-hydrophobic phase separation structure of

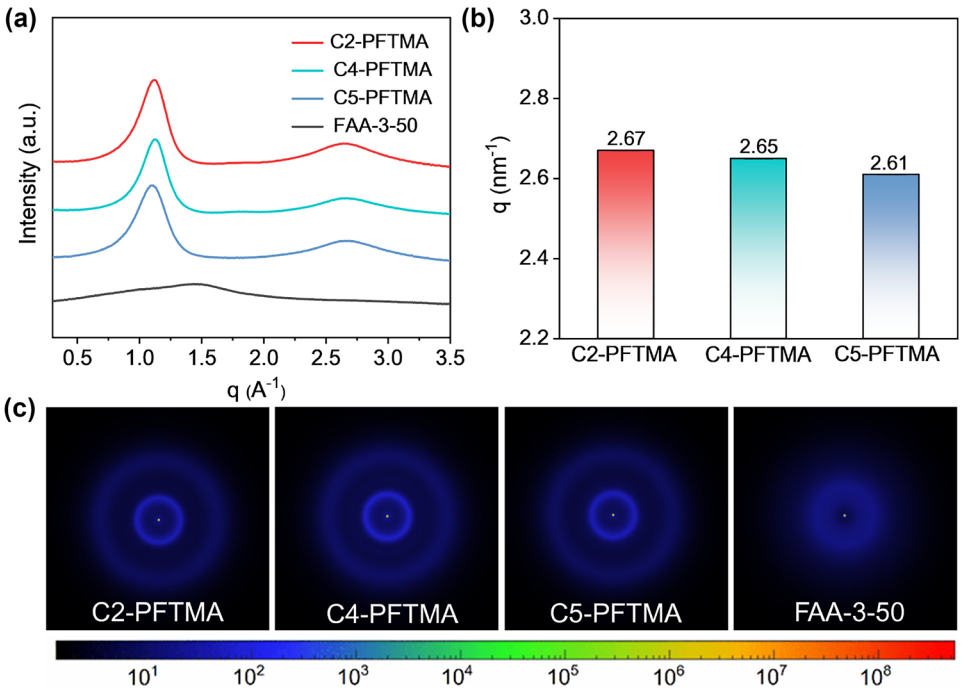

Fig. 2 **a** SAXS patterns for Cn-PFTMA and FAA-3-50 as a function of the scattering vector (q). **b** The maximum q values of Cn-PFTMA. **c** The 2D SAXS images of Cn-PFTMA and FAA-3-50

Cn-PFTMA since it was considered a well-known technique for analyzing the phase distribution of polymer materials [38]. Figure 3 exhibits AFM images of the Cn-PFTMA (a, b, c) and FAA-3-50 (d) membranes, where the dark areas represented hydrophilic cationic groups and the bright areas represented hydrophobic waters composed of polymer backbone [36]. There was a fuzzy microphase structure in the vision of the FAA-3-50 membrane. In contrast, a distinct microphase separation structure could be observed for Cn-PFTMA which could promote the establishment of well-developed ion channels. A growing average volume of ion channels was noticed for C2-PFTMA, C4-PFTMA, and C5-PFTMA, consistent with the result of SAXS. However, it was found that the increasing size of local dark regions was detrimental for the formation of ion transport networks, as a characteristic of long side chain structures. Therefore, the high degree of connectivity of the dark regions in C2-PFTMA, ion channels were interconnected, leading to a faster transport of hydroxide. This was thought to be the main source of the excellent hydroxide conductivity of the Cn-PFTMA membranes even at low IEC values.

3.3 IEC, water uptake, and hydroxide conductivity of the Cn-PFTMA membranes

The IEC value is an important indicator measuring the hydroxide conductivity and dimensional stability of AEMs, as it exerts a significant influence on water uptake. Specifically, increased IEC value delivers improved water uptake as well as hydroxide conductivity, whereas the dimensional changes along with the increased water uptake. However, AEMs often require higher IEC values because of the lower migration of the hydroxide ion [39, 40]. Thus, the balance of conductivity and dimensional stability could be better obtained by adjusting the microstructure on polymers than by enhancing IEC values [41]. The IEC values of Cn-PFTMA and FAA-3–50 were measured by reverse titration, and the calculated and experimental values corresponding to them are summarized in Table 1. C2-PFTMA, C4-PFTMA, and C5-PFTMA got a vaue of 1.20 meq g^{-1}, 1.14 meq g^{-1}, and 0.85 meq g^{-1}, respectively, which were equivalent to the calculated IEC value, indicating a complete reaction of Cn-PFTMA. In particular, the IEC value of C2-PFTMA, the highest of Cn-PFTMA, only corresponded to two-thirds of that of FAA-3-50 (1.89 meq g^{-1}).

It is known water molecules are significant carriers for the transfer of hydroxide ions [42]. Figure 4a displays the water uptake of Cn-PFTMA and FAA-3–50 under different temperatures. With the temperature rising from 30 to 80 °C, water absorption of the membranes increases consistently. Concretely, the water uptake attained 23.42%, 19.15%, and 13.78% for C2-PFTMA, C4-PFTMA, and C5-PFTMA at 80 °C, respectively, consistent with the increasing trend of IEC. Additionally, the hydration number λ absorbed per ammonium group at 80 °C was calculated for a better comparison among different membranes (Table 1). Compared with FAA-3-50, Cn-PFTMA took lower water absorption and λ values but higher hydroxide conductivity, mainly attributed to its well-hydrophilic-hydrophobic phase separation structure. Besides, the volume swelling ratio of

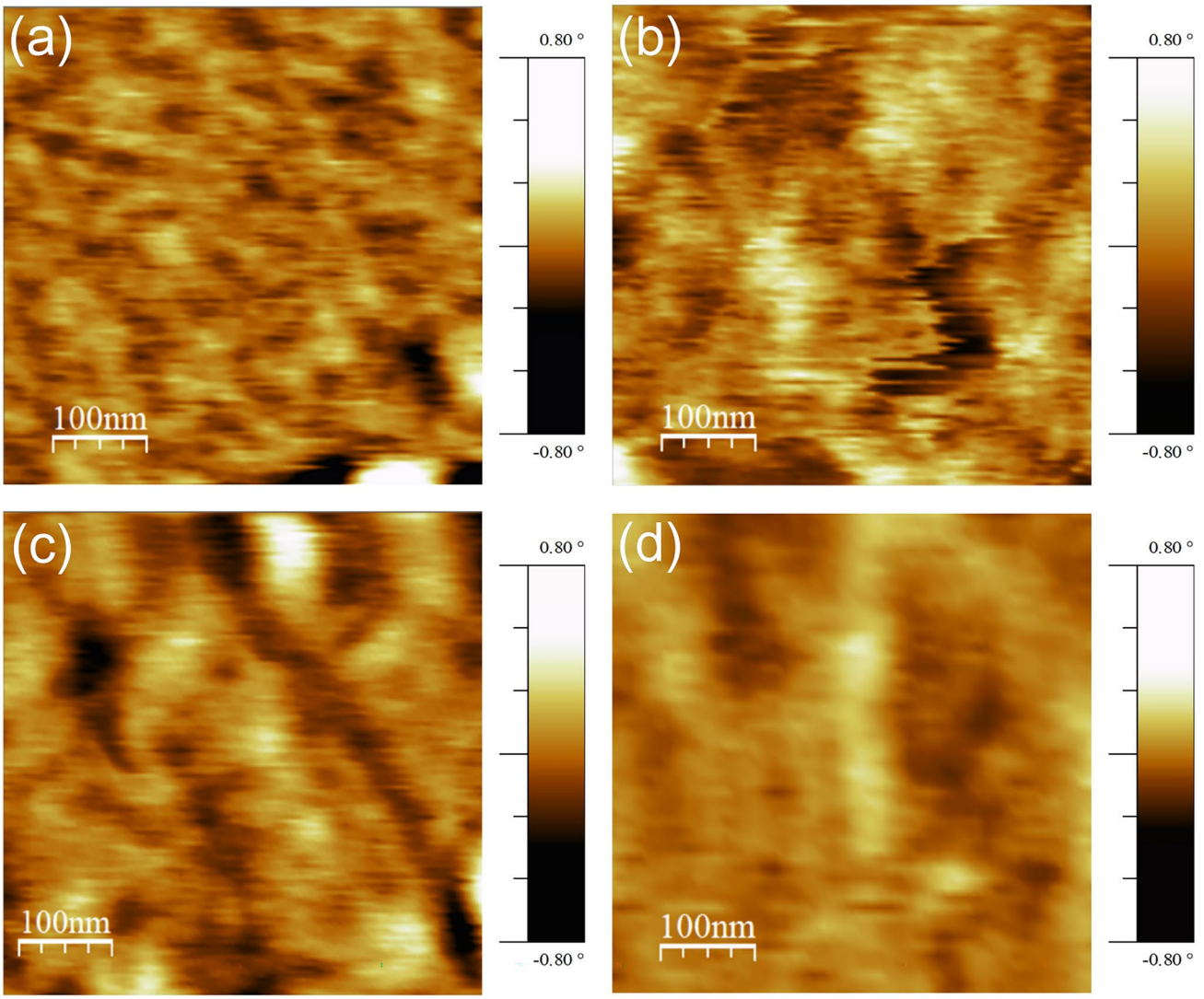

Fig. 3 AFM phase images of **a** C2-PFTMA, **b** C4-PFTMA, **c** C5-PFTMA, and **d** FAA-3-50. Scan box dimensions are 500 × 500 nm

Cn-PFTMA was followed by a temperature improvement, consistent with the trend in water uptake (Fig. 4b). It was presented that the swelling decreased from 35.08% (for C2-PFTMA) to 25.55% (for C5-PFTMA) at 80 °C along with an increase in side chain length of Cn-PFTMA in contrast with that of 131.15% for FAA-3-50, demonstrating superior dimensional stability of Cn-PFTMA. Consequently, the utilization of advanced microphase separation structures can mitigate over-absorption and swelling.

Table 1 Properties of the Cn-PFTMA membranes and FAA-3-50 membrane

Membrane code	IEC(meq g^{-1})		Water uptake (%)	Volume swelling ratio (%)	λ^c	σ_{OH^-} (mS cm^{-1})
	The[a]	EXP[b]				
C2-PFTMA	1.27	1.20	23.42	35.08	10.8	94.7
C4-PFTMA	1.25	1.14	19.15	30.23	9.3	73.5
C5-PFTMA	0.91	0.85	13.78	25.55	9.0	59.0
FAA-3-50	1.6–2.1	1.89	104.10	131.15	30.6	53.8

[a]Theoretical values

[b]Experimental values accessed from back-titration

[c]Hydration number λ acquired by $\lambda = [water\ uptake \times 1000]/[MH_2O \times IEC]$

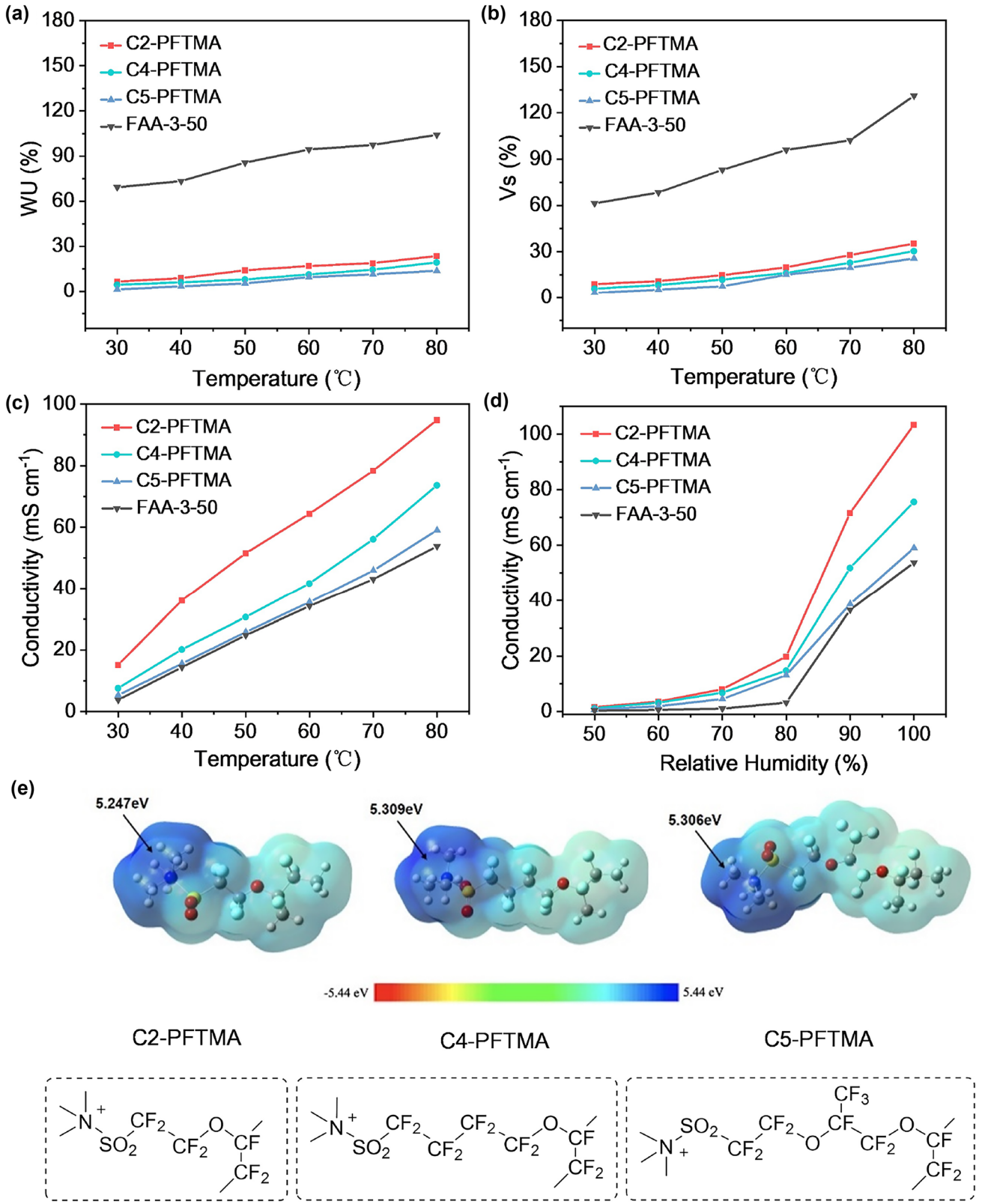

Fig. 4 Temperature dependence of **a** water uptake and **b** volume swelling ratio for the Cn-PFTMA and FAA-3-50 membranes. The hydroxide conductivities as a function of **c** temperature at 100% RH and **d** humidity at 80 °C of Cn-PFTMA and FAA-3-50. **e** ESP (surface isovalue 0.001 a.u.) of Cn-PFTMA

Hydroxide conductivity is a vital factor of AEMs. Therefore, the impact of microphase separation structure on conductivity has been thoroughly investigated [43]. The conductivity of Cn-PFTMA and FAA-3–50 was tested under different temperatures at 100% RH (Fig. 4c). Ranging from 30 to 80 °C, the hydroxide conductivity of all membranes grew concomitantly due to the high-temperature benefits of the migration of hydroxide ions. Compared with FAA-3-50, relatively excellent hydroxide conduction capacity was observed for C2-PFTMA even at lower IEC. Specifically, C2-PFTMA (IEC = 1.20 meq g^{-1}) exhibited a conductivity of 94.7 mS cm^{-1} at 80 °C, 1.8 times higher than that of FAA-3-50 (IEC = 1.89 meq g^{-1}). Meanwhile, C2-PFTMA presented the most outstanding hydroxide conductivity of Cn-PFTMA which could be attributed to the increasing of ion exchange groups and water uptake, as well as the interconnection of ion channels, which facilitated ion transport. The higher hydroxide conductivity of the C2-PFTMA membrane could also be attributed to its lower ESP (5.247 eV) (Fig. 4e) due to a less concentrated electron density around the cationic groups. As such, there was a weaker binding force between quaternary ammonium groups and hydroxide, which favored the dissociation of hydroxide [44]. As water molecules strongly influence hydroxide transport, Fig. 4d explains the dependence of conductivity on RH. The conductivity performed better under high RH conditions due to the absorption of more free water that provided a larger carrier enabling transport. Overall, Cn-PFTMA exhibited better hydroxide conductivity during the whole temperature and relative humidity compared to FAA-3-50 and low water uptake for high dimensional stability, which seemed to be attributed to the well-developed ion channel network of the Cn-PFTMA membranes.

3.4 Mechanical, thermal, and chemical stability of the Cn-PFTMA membranes

The mechanical properties and durability of AEMs must be adequate to ensure the operability of AEMWE. As illustrated in Fig. 5a, the tensile strength of C2-PFTMA, C4-PFTMA, and C5-PFTMA membranes was 29.1 MPa, 25.1 MPa, and 23.5 MPa, respectively, which decreased with the increased side chain length due to the low main chain crystallinity after annealing at high temperature. All the Cn-PFTMA membranes displayed more remarkable toughness than the commercial FAA-3-50 membrane (13.0 MPa), indicating that Cn-PFTMA could meet the requirements of AEMWE.

Thermogravimetric analysis (TGA) was conducted to assess the thermal stability of the Cn-PFTMA membranes. The results showed a similar mass loss over the temperature rise and greater heat resistance compared to the FAA-3-50 membrane (Fig. 5b). The mass loss profile of the Cn-PFTMA membranes was composed of three stages. The first stage was characterized by a 5% mass loss at around 430 °C, likely due to the decomposition of quaternary ammonium groups. The second stage saw a significant mass loss between 440 °C and 500 °C, which was attributed to the degradation of the fluoroalkyl side-chain. Lastly, the third stage was observed at around 500 °C, which was caused by the breakdown of the PTFE framework. This degradation process confirms that the Cn-PFTMA membranes are suitable for use at 70 °C [45, 46].

Density functional theory (DFT) was developed to study the effect of side chain length on the chemical stability of quaternary ammonium cations. The surface charge environment of the side chain of Cn-PFTMA is displayed in Fig. 4e; C2-PFTMA, C4-PFTMA, and C5-PFTMA attained ESP values of 5.247 eV, 5.309 eV, and 5.306 eV, respectively. It was found that the location and amount of the ether spacer had a significant impact on the ESP, as the ether spacer had a poorer electron absorption capacity than the fluoroalkyl, reducing the strong electron adsorption capacity of the fluoroalkyl side chains and increasing the electron cloud density of the cations [47]. According to this rule, the lower the ESP, the more difficult it is for a nucleophilic reagent to attack the quaternary ammonium cations, leading to a higher chemical stability in the case of C2-PFTMA.

The frontier molecular orbital theory was utilized to further explore the influence of side chains on chemical stability. The calculated LUMO energies of quaternary ammonium

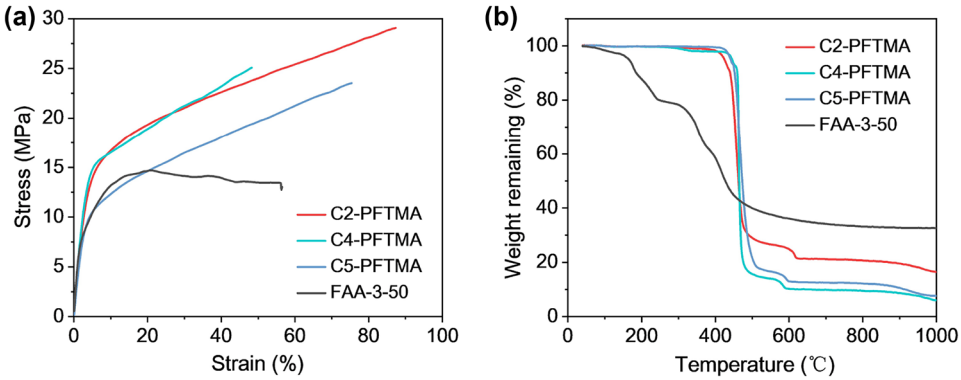

Fig. 5 **a** Stress–strain and **b** TGA curves of Cn-PFTMA and FAA-3–50

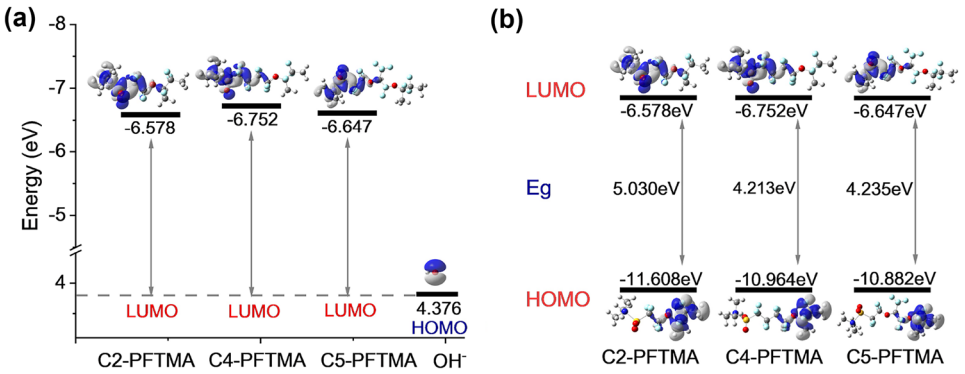

Fig. 6 **a** LUMO energies of Cn-PFTMA and HOMO energy of OH^-. **b** LUMO–HOMO energy gap plots of Cn-PFTMA

cations in C2-PFTMA, C4-PFTMA, and C5-PFTMA were – 6.578 eV, – 6.752 eV, and – 6.647 eV respectively. The higher LUMO energy of C2-PFTMA indicated a greater resistance to nucleophilic attack by OH^- compared to C4-PFTM and C5-PFTMA, which was consistent with the results of the electrostatic potential (ESP). Additionally, the LUMO–HOMO energy gap diagram (Fig. 6b) revealed a more significant LUMO–HOMO energy gap in C2-PFTMA, which would lead to increased chemical stability due to a decreased electron correlation effect.

3.5 Water electrolyzer performance of the Cn-PFTMA membranes

Considering the remarkable electrochemical properties of Cn-PFTMA, the behaviors of AEMWEs assembled with the Cn-PFTMA membranes were explored. Figures 7a and S3a display the polarization curves of Cn-PFTMA and FAA-3-50 in AEMWEs. When fed with pure water at 70 °C, a current density of 277 mA cm^{-2} at 1.9 V was acquired for the C2-PFTMA-based electrolyzer, while the AEMWE with the C4-PFTMA and C5-PFTMA membranes performed a current density of 209 mA cm^{-2} and 143 mA cm^{-2} at 1.9 V respectively, all of which were higher than that of the FAA-3-50-based one (43.5 mA cm^{-2}). This better performance could be caused by the influence of ohmic resistance, as shown in Figs. 7b and S3b; the ohmic resistance of the Cn-PFTMA-based electrolyzer increased in the order C2-PFTMA (0.31 Ω cm^2) < C4-PFTMA (0.33 Ω cm^2) < C5-PFTMA (0.48 Ω cm^2) < FAA-3-50 (0.57 Ω cm^2) at 1.9 V, consistent with current density tendency. Since the MEA is identical in composition and preparation technique, the various performances of Cn-PFTMA-based electrolyzers necessarily manifested itself in the behavior of hydroxide transport, and the membranes with higher hydroxide conductivity led to better-performance AEMWE.

Table 2 presents the hydroxide conductivity and current density of AEMWE based on recently reported AEMs. The electrochemical properties of the C2-PFTMA membrane were compared to other AEMs (No. 2–No. 9) with the IrO_2 anode and the Pt/C cathode in pure water. It was found that the C2-PTMA membrane with microphase-separated structure provided improved hydroxide conductivity at low IEC

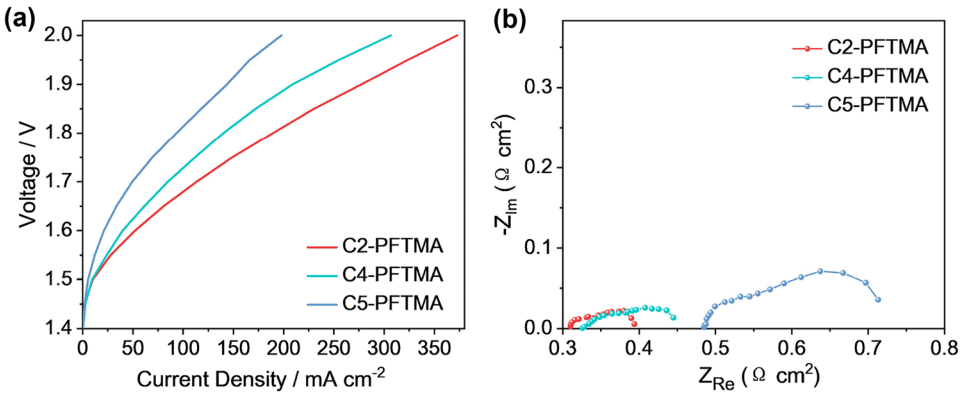

Fig. 7 **a** Polarization curves and **b** Nyquist plots for AEMWE with the Cn-PFTMA membranes. Nyquist plots were evaluated at 1.9 V

Table 2 Comparative of hydroxide conductivity and current density with other works [41, 48–54]

No.	Samples	IEC (meq g^{-1})	Hydroxide conductivity (mS cm^{-1}@°C)	T (°C)	Current density (mA cm^{-2}@V)	Ref.
1	C2-PFTMA	1.20	94.7@80	70	277@1.9	This work
2	SCPi	1.65	~53@80	50	200@1.8	[48]
3	PTP-C6	2.34	86.6@80	80	~200@1.9	[49]
4	HWU-AEM	1.86	99.4@80	60	254@1.9	[50]
5	QMter-co-Mpi-100%	2.42	66@80	50	60@2.0	[51]
6	PAES-TMI-0.25	1.85	84.35@80	80	~200@2.0	[52]
7	cPVBMP-3.0 cQPPO	2.23	160.5@80	60	210@1.8	[53]
8	TM1-MEA	N/A	N/A	70	180@1.9	[54]
9	QPC-TMA	2.31	125@70	70	~300@1.9	[41]

values and better performance in AEMWE than the data reported so far.

4 Conclusion

In summary, a series of quaternary perfluorinated anion exchange ionomers Cn-PFTMA were prepared from soluble perfluorosulfonic acid resins with different side chain lengths. The Cn-PFTMA membranes form a distinctive hydrophilic-hydrophobic phase separation structure, enabling rapid hydroxide ion transport via reliable ion channels under low IEC conditions, which avoids the reduced physical stability due to excessive water absorption and swelling triggered by high IEC, thus providing a favorable equilibrium between hydroxide transport and physical stability. Moreover, a rise in side chain length contributes to a larger hydrophilic channel volume yet reduced connectivity just as the C5-PFTMA membrane showed an enormous hydrophilic channel volume but scattered and poor connectivity, characteristic of the long chain structure. The hydroxide conductivity of the C2-PFTMA membrane with an ultra-weak IEC value of 1.20 meq g^{-1} was 94.7 mS cm^{-1} at 80 °C, consistent with the minimum ESP value calculated by DFT. More impressively, the C2-PFTMA-based electrolyzers also achieved a favorable performance of 277 mA cm^{-2}@1.9 V with pure water feed. This indicates that the construction of microphase separation structures effectively maintains a balance of the ion transport and physical stability of AEMs.

Supplementary Information The online version contains supplementary material available at https://doi.org/10.1007/s42114-023-00657-w.

Author contribution Shuhong Zheng analyzed most of the data and wrote the initial draft of the paper. Shengqiu Zhao designed the study and collected the data. Hongyun Tan, Rui Wang, and Miaoyan Zhai contributed to refining the ideas and conducting additional analyses. Haining Zhang and Huali Qin contributed to reviewing and editing and supervising the paper. Haolin Tang contributed to the central idea and finalizing this paper. Shuhong Zheng and Shengqiu Zhao contributed equally to this work. All the authors reviewed the manuscript.

Funding This work was supported by the National Natural Science Foundation of China (T2241003), National Key Research and Development Program of China (2022YFB4003500), and the Guangdong Basic and Applied Basic Research Foundation (2021B1515120072).

Declarations

Conflict of interest The authors declare no competing interests.

References

1. Pivovar B, Carmo M, Ayers K, Zhang X, O'Brien J (2016) Preface-JES focus issue on electrolysis for increased renewable energy penetration. J Electrochem Soc 163(11):Y19–Y19. https://doi.org/10.1149/2.0281611jes
2. Henkensmeier D, Najibah M, Harms C, Žitka J, Hnát J, Bouzek K (2021) Overview: state-of-the art commercial membranes for anion exchange membrane water electrolysis. J Electrochem Energ Conversion Storage 18(2). https://doi.org/10.1115/1.4047963
3. Miller HA, Bouzek K, Hnat J, Loos S, Bernäcker CI, Weißgärber T, Röntzsch L, Meier-Haack J (2020) Green hydrogen from anion exchange membrane water electrolysis: a review of recent developments in critical materials and operating conditions. Sustainable Energy Fuels 4(5):2114–2133. https://doi.org/10.1039/c9se01240k
4. Shiva Kumar S, Himabindu V (2019) Hydrogen production by PEM water electrolysis - a review. Materials Science for Energy Technologies 2(3):442–454. https://doi.org/10.1016/j.mset.2019.03.002
5. Shin DW, Guiver MD, Lee YM (2017) Hydrocarbon-based polymer electrolyte membranes: importance of morphology on ion transport and membrane stability. Chem Rev 117(16):4759–4805. https://doi.org/10.1021/acs.chemrev.6b00586
6. Varcoe JR, Atanassov P, Dekel DR, Herring AM, Hickner MA, Kohl PA, Kucernak AR, Mustain WE, Nijmeijer K, Scott K, Xu T, Zhuang L (2014) Anion-exchange membranes in electrochemical energy systems. Energy Environ Sci 7(10):3135–3191. https://doi.org/10.1039/c4ee01303d
7. Li S, Zhu X, Liu D, Sun F (2018) A highly durable long side-chain polybenzimidazole anion exchange membrane for AEMFC. J Membr Sci 546:15–21. https://doi.org/10.1016/j.memsci.2017.09.064
8. Wang X, Li J, Chen W, Pang B, Liu Y, Guo Y, Wu X, Cui F, He G (2021) Polybenzimidazole ultrathin anion exchange membrane with comb-shape amphiphilic microphase networks

for a high-performance fuel cell. ACS Appl Mater Interfaces 13(42):49840–49849. https://doi.org/10.1021/acsami.1c12570
9. Liu W, Liu L, Liao J, Wang L, Li N (2017) Self-crosslinking of comb-shaped polystyrene anion exchange membranes for alkaline fuel cell application. J Membr Sci 536:133–140. https://doi.org/10.1016/j.memsci.2017.05.006
10. Lin C, Liu X, Yang Q, Wu H, Liu F, Zhang Q, Zhu A, Liu Q (2019) Hydrophobic side chains to enhance hydroxide conductivity and physicochemical stabilities of side-chain-type polymer AEMs. J Membr Sci 585:90–98. https://doi.org/10.1016/j.memsci.2019.04.066
11. Li S, Du S, Xie N, Zhang T, Xu Y, Ning X, Chen P, Chen X, An Z (2022) Imidazole-functionalized multiquaternary side-chain polyethersulfone anion-exchange membrane for fuel cell applications. ACS Applied Energy Materials 5(8):10023–10033. https://doi.org/10.1021/acsaem.2c01647
12. Niu M, Zhang C, He G, Zhang F, Wu X (2019) Pendent piperidinium-functionalized blend anion exchange membrane for fuel cell application. Int J Hydrogen Energy 44(29):15482–15493. https://doi.org/10.1016/j.ijhydene.2019.04.172
13. You W, Noonan KJT, Coates GW (2020) Alkaline-stable anion exchange membranes: a review of synthetic approaches. Progress in Polymer Science 100:101177. https://doi.org/10.1016/j.progpolymsci.2019.101177
14. Tanaka M, Fukasawa K, Nishino E, Yamaguchi S, Yamada K, Tanaka H, Bae B, Miyatake K, Watanabe M (2011) Anion conductive block poly(arylene ether)s: synthesis, properties, and application in alkaline fuel cells. J Am Chem Soc 133(27):10646–10654. https://doi.org/10.1021/ja204166e
15. Kusoglu A, Weber AZ (2017) New insights into perfluorinated sulfonic-acid ionomers. Chem Rev 117(3):987–1104. https://doi.org/10.1021/acs.chemrev.6b00159
16. Kim JQ, So S, Kim H-T, Choi SQ (2020) Highly ordered ultrathin perfluorinated sulfonic acid ionomer membranes for vanadium redox flow battery. ACS Energy Lett 6(1):184–192. https://doi.org/10.1021/acsenergylett.0c02089
17. Zeng Z, Song R, Zhang S, Han X, Zhu Z, Chen X, Wang L (2021) Biomimetic N-doped graphene membrane for proton exchange membranes. Nano Lett 21(10):4314–4319. https://doi.org/10.1021/acs.nanolett.1c00813
18. Oshiba Y, Tomatsu J, Yamaguchi T (2018) Thin pore-filling membrane with highly packed-acid structure for high temperature and low humidity operating polymer electrolyte fuel cells. J Power Sources 394:67–73. https://doi.org/10.1016/j.jpowsour.2018.05.013
19. Di Noto V, Zawodzinski TA, Herring AM, Giffin GA, Negro E, Lavina S (2012) Polymer electrolytes for a hydrogen economy. Int J Hydrogen Energy 7(37):6120–6131. https://doi.org/10.1016/j.ijhydene.2012.01.080
20. Park AM, Owczarczyk ZR, Garner LE, Yang-Neyerlin AC, Long H, Antunes CM, Sturgeon MR, Lindell MJ, Hamrock SJ, Yandrasits M, Pivovar BS (2017) Synthesis and characterization of perfluorinated anion exchange membranes. ECS Trans 80(8):957–966. https://doi.org/10.1149/08008.0957ecst
21. Kreuer KD, Paddison SJ, Spohr E, Schuster M (2004) Transport in proton conductors for fuel-cell applications: simulations, elementary reactions, and phenomenology. Chem Rev 104(10):4637–4678. https://doi.org/10.1021/cr020715f
22. M-sJ J, Arges CG, Ramani V (2011) A perfluorinated anion exchange membrane with a 1,4-dimethylpiperazinium cation. J Mater Chem 21(17):6158–6160. https://doi.org/10.1039/c1jm10320b
23. Nguyen Q-M, Jung SY, Hwang JP, Ahn J, Lim JH, Jang W, Lee CH (2020) Perfluorinated anion exchange membranes for alkaline water electrolysis. ECS Trans 98(9):703–712. https://doi.org/10.1149/09809.0703ecst
24. Liu X, Gao H, Chen X, Hu Y, Pei S, Li H, Zhang Y (2016) Synthesis of perfluorinated ionomers and their anion exchange membranes. J Membr Sci 515:268–276. https://doi.org/10.1016/j.memsci.2016.05.062
25. Salerno HLS, Elabd YA (2013) Anion exchange membranes derived from nafion precursor for the alkaline fuel cell: effect of cation type on properties. J Appl Polym Sci 127(1):298–307. https://doi.org/10.1002/app.37874
26. Liu H, Guo L, Liu M, Chen H, Han W, Bian H, Tian X, Wang C, Guo Z, Sun J (2021) Water management simulation of proton exchange membrane fuel cells with micro-ribs based on volume of fluid model. ES Energy & Environment 15:45–55. https://doi.org/10.30919/esee8c530
27. Wang B, Sun X, Xie X, Wang J, Li L, Jiao K (2021) Experimental investigation of a novel cathode matrix flow field in proton exchange membrane fuel cell. ES Energy & Environment 12:95–107. https://doi.org/10.30919/esee8c422
28. Perusich SA (2011) Ftir equivalent weight determination of perfluorosulfonate polymers. J Appl Polym Sci 120(1):165–183. https://doi.org/10.1002/app.32871
29. Lowry SR, Mauritz KA (2002) An investigation of ionic hydration effects in perfluorosulfonate ionomers by Fourier transform infrared spectroscopy. J Am Chem Soc 102(14):4665–4667. https://doi.org/10.1021/ja00534a017
30. Liu X, Chen X, Hu Y, Gong T, Li H, Zhang Y (2017) Ionic-liquid-functionalized graphene nanoribbons for anion exchange membrane fuel cells. J Electrochem Soc 164(4):F433–F440. https://doi.org/10.1149/2.0141706jes
31. Öztürk N, Bahçeli S (2006) Ft-ir spectroscopic study of 1,3-diaminopropane adsorbed on type a, x and y zeolites. Zeitschrift für Naturforschung A 61(7–8):399–401. https://doi.org/10.1515/zna-2006-7-814
32. Bonizzoni S, Stilli P, Lohmann-Richters F, Oldani C, Ferrara C, Papagni A, Beverina L, Mustarelli P (2021) Facile chemical modification of Aquivion® membranes for anionic fuel cells. ChemElectroChem 8(12):2231–2237. https://doi.org/10.1002/celc.202100382
33. Wang Z, Tang H, Li J, Zeng Y, Chen L, Pan M (2014) Insight into the structural construction of a perfluorosulfonic acid membrane derived from a polymeric dispersion. J Power Sources 256:383–393. https://doi.org/10.1016/j.jpowsour.2014.01.096
34. Wu X, Chen W, Yan X, He G, Wang J, Zhang Y, Zhu X (2014) Enhancement of hydroxide conductivity by the di-quaternization strategy for poly(ether ether ketone) based anion exchange membranes. Journal of Materials Chemistry A 2(31):12222–12231. https://doi.org/10.1039/c4ta01397b
35. Li G, Shen R, Hu S, Wang B, Algadi H, Wang C (2022) Norbornene-based acid–base blended polymer membranes with low ion exchange capacity for proton exchange membrane fuel cell. Advanced Composites and Hybrid Materials 5(3):2131–2213. https://doi.org/10.1007/s42114-022-00559-3
36. Yang J, Tong L, Alsubaie AS, Mahmoud KH, Guo Y, Liu L, Guo L, Sun Z, Wang C (2022) Hybrid proton exchange membrane used in fuel cell with amino-functionalized metal-organic framework in sulfonated polyimide to construct efficient ion transport channel. Advanced Composites and Hybrid Materials 5(2):834–842. https://doi.org/10.1007/s42114-022-00469-4
37. Shin SH, Nur PJ, Kodir A, Kwak DH, Lee H, Shin D, Bae B (2019) Improving the mechanical durability of short-side-chain perfluorinated polymer electrolyte membranes by annealing and physical reinforcement. ACS Omega 4(21):19153–19163. https://doi.org/10.1021/acsomega.9b02436
38. Wang Z, Tang H, Zhang H, Lei M, Chen R, Xiao P, Pan M (2012) Synthesis of nafion/CeO_2 hybrid for chemically durable proton exchange membrane of fuel cell. J Membr Sci 421–422:201–210. https://doi.org/10.1016/j.memsci.2012.07.014
39. Cha MS, Lee JY, Kim T-H, Jeong HY, Shin HY, Oh S-G, Hong YT (2017) Preparation and characterization of crosslinked anion exchange membrane (AEM) materials with poly(phenylene ether)-based short

hydrophilic block for use in electrochemical applications. J Membr Sci 530:73–83. https://doi.org/10.1016/j.memsci.2017.02.015
40. Lee JY, Yu DM, Kim T-H, Yoon SJ, Hong YT (2015) Multi-block copolymers based on poly(p-phenylene)s with excellent durability and fuel cell performance. J Membr Sci 492:209–219. https://doi.org/10.1016/j.memsci.2015.04.013
41. Cha MS, Park JE, Kim S, Han S-H, Shin S-H, Yang SH, Kim T-H, Yu DM, So S, Hong YT, Yoon SJ, Oh S-G, Kang SY, Kim O-H, Park HS, Bae B, Sung Y-E, Cho Y-H, Lee JY (2020) Poly(carbazole)-based anion-conducting materials with high performance and durability for energy conversion devices. Energy Environ Sci 13(10):3633–3645. https://doi.org/10.1039/d0ee01842b
42. Zhao S, Wang R, Tian T, Liu H, Zhang H, Tang H (2022) Self-assembly-cooperating in situ construction of MXene–CeO_2 as hybrid membrane coating for durable and high-performance proton exchange membrane fuel cell. ACS Sustainable Chemistry & Engineering 10(13):4269–4278. https://doi.org/10.1021/acssuschemeng.2c00087
43. Pan Y, Jiang K, Sun X, Ma S, So Y-M, Ma H, Yan X, Zhang N, He G (2021) Facilitating ionic conduction for anion exchange membrane via employing star-shaped block copolymer. Journal of Membrane Science 630:119290. https://doi.org/10.1016/j.memsci.2021.119290
44. Zhang J, Zhang K, Liang X, Yu W, Ge X, Shehzad MA, Ge Z, Yang Z, Wu L, Xu T (2021) Self-aggregating cationic-chains enable alkaline stable ion-conducting channels for anion-exchange membrane fuel cells. Journal of Materials Chemistry A 9(1):327–337. https://doi.org/10.1039/d0ta11011f
45. De Almeida SH, Kawano Y (1999) Thermal behavior of Nafion membranes. J Therm Anal Calorim 58(3):569–577. https://doi.org/10.1023/a:1010196226309
46. Chempath S, Einsla BR, Pratt LR, Macomber CS, Boncella JM, Rau JA, Pivovar BS (2008) Mechanism of tetraalkylammonium headgroup degradation in alkaline fuel cell membranes. The Journal of Physical Chemistry C 112(9):3179–3182. https://doi.org/10.1021/jp7115577
47. Zhang F, Li T, Chen W, Wu X, Yan X, Xiao W, Zhang Y, Wang X, He G (2021) Highly stable electron-withdrawing CO link-free backbone with branched cationic side chain as anion exchange membrane. Journal of Membrane Science 62:119052. https://doi.org/10.1016/j.memsci.2021.119052
48. Chu X, Shi Y, Liu L, Huang Y, Li N (2019) Piperidinium-functionalized anion exchange membranes and their application in alkaline fuel cells and water electrolysis. Journal of Materials Chemistry A 7(13):7717–7727. https://doi.org/10.1039/c9ta01167f
49. Liu L, Bai L, Liu Z, Miao S, Pan J, Shen L, Shi Y, Li N (2023) Side-chain structural engineering on poly(terphenyl piperidinium) anion exchange membrane for water electrolysers. Journal of Membrane Science 665:121135. https://doi.org/10.1016/j.memsci.2022.121135
50. Xu Z, Wan L, Liao Y, Wang P, Liu K, Wang B (2021) Anisotropic anion exchange membranes with extremely high water uptake for water electrolysis and fuel cells. Journal of Materials Chemistry A 9(41):23485–23496. https://doi.org/10.1039/d1ta06579c
51. Yan X, Yang X, Su X, Gao L, Zhao J, Hu L, Di M, Li T, Ruan X, He G (2020) Twisted ether-free polymer based alkaline membrane for high-performance water electrolysis. Journal of Power Sources 480:228805. https://doi.org/10.1016/j.jpowsour.2020.228805
52. Qian J, Wang C, Zhang X, Zhao X, Li J, Ren Q (2022) Dense 1,2,4,5-tetramethylimidazolium-functionlized anion exchange membranes based on poly(aryl ether sulfone)s with high alkaline stability for water electrolysis. Int J Hydrogen Energy. https://doi.org/10.1016/j.ijhydene.2022.11.258
53. Zeng L, Yuan W, Ma X, He Q, Zhang L, Wang J, Wei Z (2022) Dual-cation interpenetrating polymer network anion exchange membrane for fuel cells and water electrolyzers. Macromolecules 55(11):4647–4655. https://doi.org/10.1021/acs.macromol.1c02600
54. Kang SY, Park JE, Jang GY, Kim O-H, Kwon OJ, Cho Y-H, Sung Y-E (2022) High-performance and durable water electrolysis using a highly conductive and stable anion-exchange membrane. Int J Hydrogen Energy 47(15):9115–9126. https://doi.org/10.1016/j.ijhydene.2022.01.002